Experimental focusing shocklike dynamics in a nonlocal optical stochastic Kerr medium

A. Aleksanyan,[1] H. Louis,[1] J. F. Henninot,[2] and E. Louvergneaux[1,*]

[1]*Universite Lille, CNRS, UMR 8523 - PhLAM - Physique des Lasers Atomes et Molécules, F-59000 Lille, France*

[2]*Universite Artois, CNRS, UMR 8181 - UCCS - Unite de Catalyse et de Chimie du Solide, F-62307 Lens Cedex, France*

(Received 24 August 2020; accepted 8 January 2021; published 3 February 2021)

We experimentally study the propagating of an optical intensity jump discontinuity in a *nonlocal* stochastic Kerr *focusing* nematic liquid crystal cell. We show both theoretically and experimentally that nonlocality opens a route towards beam steering in our system. Indeed, the discontinuity trajectory follows a curve that bends with the injected power. Despite the stochastic nature of the medium and the constant presence of transverse instabilities, the development of a focusing shocklike dynamics is shown to survive. The distance Z_s for the *focusing* shock to occur follows a power law with the beam power P according to $Z_s \propto P^{\chi}$, with $\chi = -4/3$, as for shock dynamics in self-defocusing media.

DOI: 10.1103/PhysRevE.103.022701

I. INTRODUCTION

Any physics student from wave optics class has heard about the phenomenon of diffraction, i.e., varying when the wave envelope varies during propagation. They also know that this effect is embedded in Maxwell's equations, and the necessary condition for this phenomenon to occur is for the field envelope to depend on the spatial coordinates. This is *linear diffraction*. However, an additional term appears in the wave propagation equation if the wave propagates in nonlinear media. This term accounts for the medium polarization and contains the nonlinear part of the index of the medium. If the wave envelope injected into the medium has no transverse spatial dependence (ideal plane wave), no linear diffraction is observed, but diffraction can still occur providing that the nonlinearity varies with space. This is *nonlinear diffraction*, a notion that every physics student has not heard of unless they have pursued a course in nonlinear optics. Thus there are two cases where an optical beam propagating through a nonlinear medium experiences diffraction, either (i) the initial beam has a structured profile (amplitude and/or phase varying with space) and the nonlinear medium is spatially homogeneous, then the beam linearly diffracts through the nonlinear medium, or (ii) the initial beam is assimilated to a plane wave but the nonlinear medium is spatially structured so that nonlinear diffraction is achieved during propagation. The nonlinear diffraction was first introduced and evidenced by Freund using the spatially periodic modulation of the dielectric susceptibility of NH4CL [1]. Such material structuring will be later implemented for the realization of photonic lattices [2] and lead to novel nonlinear phenomena [3–6]. The most documented studies on nonlinear optical propagation deal with the above-mentioned first situation, that is, an initial beam linearly diffracting along the propagation through a spatially homogeneous nonlinear medium, first introduced by Askaryan [7]. This is the main core of nonlinear optics for beam propagation, and this article belongs to this category.

Competition or rather "cohabitation" between linear diffraction and nonlinearity has been the subject of an extensive amount of publications. Localization through solitary waves [8–10] or self-similar structures [11–13], modulational instability (also called filamentation) [14–16], wave singularities such as vortices [17], shock waves [18–20], and wave collapse [21,22] are some of the manifestations of such dynamics. We are interested in the nonlinear propagation of an optical amplitude jump discontinuity (between two uniform values of the initial data) through nonlinear *focusing* media. This problem belongs to the class of Riemann problems [23,24]. A Riemann problem [25] classically refers to the initial value problem for a transverse unidimensional system associated with hyperbolic equations consisting of two constant states with a step at the origin. When the initial wave amplitude is steplike, the terminology dam break is used, in analogy with dam break flows in hydrodynamics. This situation has been extensively studied in shallow water for the regularization of initial discontinuities via the emergence of dispersive shock waves (undular bores) when dissipation is negligible compared to dispersion [26]. Shock dynamics was later evidenced in nonlinear optics, when the nonlinearity is of *defocusing* type, in temporal systems [27,28] as well as in spatial ones [19]. On the other hand, the dynamics radically changes when the nonlinearity is of *focusing* nature. The equations become elliptic, and hence a shock boundary condition is ill posed, associated with no long-term undular bore solution but modulational instability. In optics it is predicted that for a focusing nonlinearity whose response is nonlocal, the shock prevails over modulational instability [20], and focusing dispersive dam break flows emerge [29]. Wan *et al.* experimentally demonstrated in local focusing media that using a partially coherent beam suppresses modulational instability but leads to a shock followed by spatial dispersive waves with negative pressure [30]. Thus there are scant publications and almost no experimental study of shock dynamics for an optical beam propagating through *focusing*

*eric.louvergneaux@univ-lille.fr

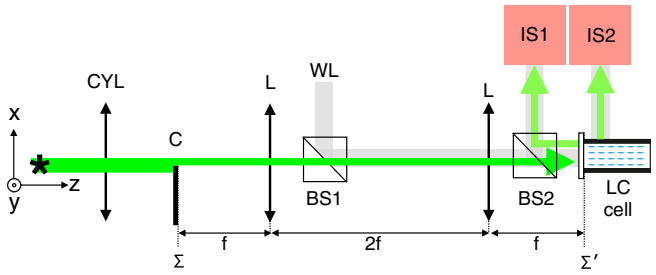

FIG. 1. Experimental setup: CYL - cylindrical lens with $f =$ 75-mm focal length, C - light cutter, L - plano-concave lenses with $f = 100$-mm focal length, BS1,BS2 - beam splitters. IS1 - imaging system composed of a 10X, NA $= 0.25$ microscope objective (Olympus) and a camera (Thorlabs CMOS camera, 10bit). BS2 - an imaging system composed of a 5X, NA $= 0.1$ microscope objective (Mitutoyo) mounted on a lens tube with $f = 200$ mm focal length and a camera (Thorlabs).

and *nonlocal* nonlinear media. This is the motivation of this study. We experimentally explore the propagation of an optical jump discontinuity in a nonlocal focusing medium which in addition is stochastic, namely, a transverse unidimensional nematic liquid crystal cell.

II. EXPERIMENTAL SETUP

Our experimental setup follows the same strategy as presented in [15]. A steplike intensity beam profile is injected into a transverse unidimensional liquid crystal (LC) cell (Fig. 1). Such a Heaviside-like profile is prepared by focusing the Gaussian beam by a cylindrical lens (CYL) onto a thin metallic blade with a sharp edge. A $4f$ imaging system is constructed via two $f = 100$-mm lenses (L) to image the light profile from the plane Σ of the cutter (C) to the entrance plane Σ' of the LC cell. The cell is mounted on a three-dimensional stage and additional rotating stages, allowing for precise adjustments via translations and rotations in any direction. To ensure that there is no prepropagation in air at the cell entrance, a series of videos of the injected probe beam are recorded for different locations z of the cell. These videos are averaged over 20-s acquisition time to reveal the possible air diffraction pattern and adjust the entrance of the cell Σ' with the plane Σ of the cutter. The single-mode frequency doubled $Nd^{+3} : Y\,V\,O_4$ ($\lambda_0 = 532$ nm) laser with electric field A is linearly polarized along the x axis initially perpendicular to the extraordinary axis of LC molecules. The input laser beam radii at the entrance of the cell, measured via a camera beam profiler (Thorlabs BC106N-VIS/M), are $\omega_x \approx 11.5\ \mu$m and $\omega_y \approx 960\ \mu$m (in the cutter plane). Thus no more than one filament can form in the vertical x direction. The nonlinear medium is a E7 nematic LC of 75-μm thickness sandwiched between two glass substrates with planar (parallel to the walls) anchoring conditions. The entrance of the cell is closed by a glass substrate with a planar anchoring condition to avoid depolarizing effects during beam injection. A white light imaging system (WL+IS1 on Fig. 1) is constructed to image the plane Σ' along with the injected one-dimensional beam profile, insuring that the latter is parallel to the walls of the LC cell. The propagation evolution of the beam is tracked via imaging system IS2 using the scattered light in the x direction. The propagating optical field is scattered by LC molecule fluctuations depending on director axis orientation, input field polarization, and observation direction [31,32]. It is not a direct image of the optical field but of its scattering by the refractive index profile. However, as in all studies on optical beam propagation through nematic LCs, it allows for qualitative analysis of the dynamics.

III. GOVERNING EQUATIONS

The model describing the nonlinear propagation dynamics in such complex media is governed by a system of coupled equations for the optical reorientation angle θ of the LC molecules and the light envelope amplitude A [33], such that

$$\gamma \frac{\partial \theta}{\partial t} = K_2 \frac{\partial^2 \theta}{\partial y^2} + C_{1T} A^2 \sin(2\theta) + \sqrt{\epsilon}\xi\,, \tag{1}$$

$$0 = -2ik_0 n_\perp \frac{\partial A}{\partial z} + \frac{\partial^2 A}{\partial y^2} + k_0^2 n_a^2 \sin(\theta)^2 A + ik_0 n_\perp \beta A, \tag{2}$$

where γ is viscosity, K_2 is the Frank's twist elastic constant, $n_a = n_\parallel - n_\perp$ is the optical anisotropy with $n_\parallel/n_\perp$ being the extraordinary/ordinary indices, $C_{1T} = \epsilon_0 n_a^2/4$, k_0 is the laser wave number, and β are losses. ϵ is the intensity of the thermal noise source term ξ, which is Gaussian and δ correlated [34]. At third order in θ, the dimensionless form of Eqs. (1) and (2) is

$$\begin{cases} \frac{\partial \psi}{\partial T} = \sigma_0^2 \frac{\partial^2 \psi}{\partial Y^2} + 2|a|^2\psi + \sqrt{\eta}\xi \\ i\frac{\partial a}{\partial Z} = \frac{1}{2}\frac{\partial^2 a}{\partial Y^2} + \frac{1}{C_a^2}\psi^2 a + i\frac{\alpha}{2}a \end{cases}, \tag{3}$$

where the following scalings are introduced: optical field A with respect to the optical Fréedericksz threshold is scaled as $A_{Fr} = \pi/L\sqrt{K_3/C_{1T}}$, such that $a = A/A_{Fr}$, L being the cell thickness and K_3 the bend elastic constant. $Y = y/(\sqrt{2}w_y)$, $Z = z/(2k_0 n_\perp w_y^2)$, $T = tK_3\pi^2/(\gamma L^2)$, $\psi = \theta w_y^2 k_0^2 n_a^2$. $\alpha = 2k_0 n_\perp w_y^2 \beta$, $C_a = w_y^2 k_0^2 n_a^2$, $\sqrt{\eta} = \sqrt{\varepsilon}L^2 C_a/(\pi^2 K_2)$. $\sigma_0 = \frac{L}{\pi w_y}\sqrt{\frac{K_2}{2K_3}}$ accounts for the degree of nonlocality.

It is worth mentioning that such a system of equations Eq. (3), even for stationary, deterministic, and lossless conditions, is fundamentally different from the *local* nonlinear Schrödinger equation usually referred to study shock problems in optics [24,30] as well as in hydrodynamics [23]; hence different dynamics is anticipated.

IV. NUMERICAL RESULTS FOR AN "IDEAL" STATIONARY NOISELESS AND LOSSLESS SYSTEM

First, numerical simulations are performed to get insight into possible nonlinear dynamics. Figure 2(b) depicts the spatiotemporal evolution of the y-transverse profile of the initially steplike optical intensity $|A|^2$ after $z = 1.2$ mm propagation for Eqs. (1) and (2) in the *local limit*, that is, $K_2 = 0$, without noise nor losses ($\epsilon = 0$ and $\beta = 0$) and for an initial amplitude value of the optical field at $z = 0$, leading to focusing shock. Apart from the oscillatory wave regularizing the discontinuity, the evolution with time stays stationary even at the early stage of the steepening (as also visible in [30]). On the contrary, taking into account for the nonlocal response of the nonlinearity

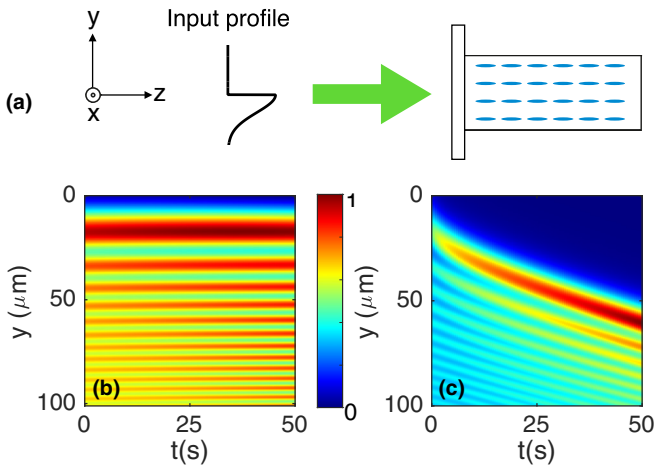

FIG. 2. (a) Steplike Gaussian intensity profile injected in the LC cell. Spatiotemporal evolution of the beam transverse profile after $z = 1.2$-mm propagation for (b) the local ($K_2 = 0$) and (c) nonlocal ($K_2 = 6.57 \times 10^{-12}$ N) cases. Both profiles are normalized to their maximum values. (b) A = 5000 and (c) A = 31 250. $\epsilon = 0$, $\beta = 0$, $n_\parallel = 1.7589$, $n_\perp = 1.5269$, $\lambda_0 = 532 \times 10^{-9}$ m, and $\omega_y \approx 960$ μm.

($K_2 = 6.57 \times 10^{-12}$ N) gives a radically different dynamics [Fig. 2(c)]. The leading edge of the oscillatory wave drifts with time to the highest intensity side. The whole transverse structure is steered during the propagation to the highest intensity value by more than 50 μm in the example of Fig. 2(c). Thus all-optical beam steering is evidenced owing to the nonlocal nature of our system. Experimentally, (i) the intrinsic thermal fluctuations are known to affect the dynamics [34] and (ii) the scattering losses are relatively high ($\beta \sim 600$ m^{-1}), so we expect competition between shock dynamics and filamentation (absent in the ideal case of simulations depicted in Fig. 2) as pointed out in [20,29] and wonder if shock dynamics can still survive in our stochastic system.

V. EXPERIMENTAL RESULTS

Typical experimental propagation evolution of the initial optical intensity jump discontinuity with increasing nonlinearity is displayed in Figs. 3(a)–3(c). The dynamics exhibits a continuous evolution of the fine structure of the propagating optical pattern due to the stochastic nature of the nonlinear medium as described in [35]. However, its global shape remains quasistationary after a transient setup time. Thus videos of the dynamics are recorded (20-s duration at 5 fps) with a 10-bit depth dynamic range to extract corresponding averaged images representative of the global shape of the propagating structure, as presented in Figs. 3(a)–3(c). The acquisition time of the camera is automatically adjusted by the software to get unsaturated videos taking into account eventual light pinning or saturated pixels due to cell impurities. The first 200 μm of propagation are not reported on experimental plots (i) to avoid scattered signals from the optical field injection at the entrance of the cell and mainly (ii) to allow for the input light to transfer its boundary condition discontinuity on the LC molecule distribution, that is, to the medium refractive index. This latter point is crucial, since our system is described by a set of two

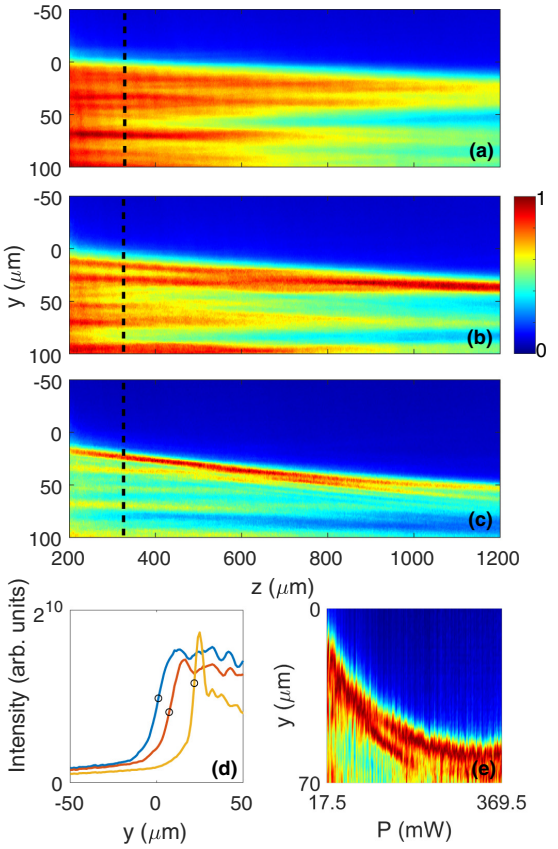

FIG. 3. Spatial evolution of the initial intensity jump discontinuity vs propagating distance z for increasing laser power measured before the sample entrance, namely, (a) $P = 17.5$ mW, (b) $P = 73.8$ mW, and (c) $P = 193.5$ mW. The intensity profiles are normalized to their maximum values. (d) Transverse intensity profiles at $z = 354$ μm propagating distance [dotted lines on (a), (b), and (c)] for the three power values of diagrams (a), (b), and (c). Black circles on (d) locate the scattered light intensity discontinuity Y_S (see text for definition). (e) Evolution of the intensity profile at $z = 1200$ μm vs the injected light power P; the transverse profiles collected for each value of P are normalized to 1 in order the render the image readable. All data are averaged over 20 s of dynamics.

coupled equations [Eqs. (1) and (2)], and the initial boundary condition is only applied to the light envelope amplitude A, not to the optical reorientation angle θ of the LC molecules. In usual setups where the Riemann problem is studied, only one variable accounts for the propagation dynamics of the system (e.g., nonlinear Schrödinger equation or Korteweg–de Vries equation) and the initial condition is applied to this variable [28,36,37]. Also, the scattered light recorded by the camera IS2 is a result of the LC index distribution that has no initial jump discontinuity at $z = 0$ but will only acquire it over the early stage of propagation ($100 - 200$ μm).

A. Bending of the edge trajectory

Three values of the injected optical power P, representative of the dynamics of interest, are shown on Figs. 3(a)–3(c), namely, $P = 17.5$ mW, $P = 193.5$ mW, and $P = 286.7$ mW. For the lowest power [Fig. 3(a)] the regime is dominated

by linear diffraction, and the observed small deviation experienced by the discontinuity is attributed to linear Fresnel diffraction. The dynamics drastically changes when increasing the laser power with a transverse shift of the sharp edge [Figs. 3(b) and 3(c)]. The edge steering is clearly evidenced on Fig. 3(d) through the transverse intensity profiles plotted at a fixed propagation distance, namely, $z = 354\ \mu$m, for the three powers of Figs. 3(a)–3(c). A shift of $\sim 20\ \mu$m is obtained after only 354-μm propagation. The 0 reference of the transverse y axis is fixed by the location of the discontinuity at $z = 200\ \mu$m in the linear regime (that is, $P = 17.5$ mW). Figure 3(d) also evidences the steepening of the edge with increasing power. For the highest depicted power [Fig. 3(c)], the reached transverse steering at 1.2 mm propagation distance from the cell entrance is at least 40 μm, that is larger than 33 mrad. Such beam deviation is low compared with the 0.2-rad value reported in studies [38,39]. However, our strategy does not require any external factors such as a second beam or a mechanical translation of the cell and is solely related to the intrinsic nonlocal nature of the nonlinearity. The amount of steering obtained after 1.2-mm propagation versus the input beam power P is plotted in Fig. 3(e), clearly demonstrating a power dependence of the sharp edge position shift. For a quantitative analysis of this nonlinear beam deviation, the transverse position Y_s of the intensity discontinuity is tracked. As an example, Y_s is marked by a black circle on the profiles of Fig. 3(d). At a given propagating distance z, Y_s corresponds to the abscissa of the maximum of the transverse intensity steepness calculated as $S_z(y) = (\partial|A|^2/\partial y)|_z$. The measurement of this dependence brings out a power law for Y_s as depicted in Fig. 4(d), namely, $Y_s \propto P^{\frac{1}{25}}$.

Experimental results of Fig. 3 show that the beam steering predicted in Fig. 2 is a robust phenomenon with respect to noise and scattering losses. On the other hand, Fig. 3 does not show focusing dispersive waves as in Figs. 2(b) and 2(c). A numerical study would be necessary to identify the effects of noise, losses, and, e.g., nonlinearity saturation effects on the emergence of the focusing dispersive oscillating structure. This is out of the scope of this article, since the high transverse spatial resolution required to perform numerical simulations on such a wide beam profile requires many weeks of computing to reach the stationary state in the deterministic case. This is why in this work we do not directly contrast our experimental results with numerical ones, based on Eqs. (1) and (2). We want to point out that transverse instabilities, in the form of modulational instabilities, starting from the early stage of propagation (so not the focusing dispersive dam break flows) are always present even for the "linear regime" of Fig. 3(a) as mentioned in [40]. The averaged pictures of Figs. 3(a) and 3(c) do not emphasize them, since their transverse location and periodicity are wandering with time [35] and are washed out by the averaging process. Further study would be necessary to identify these short wavelength instabilities with noise-sustained modulational instability [15] or other stochastic resonance behavior [41].

B. Focusing shocklike dynamics

Let us check now for shocklike dynamics. Focusing shock results from the underlying mechanism of the wave steepening

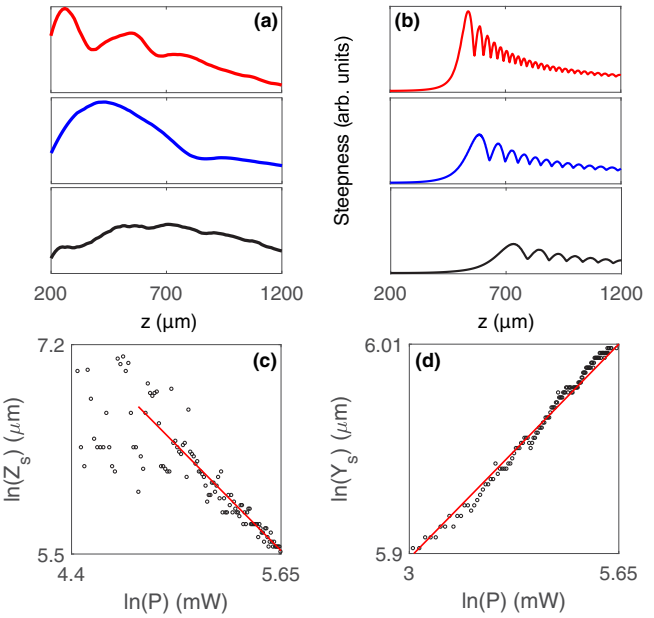

FIG. 4. (a) Typical experimental maximum transverse steepening $S_{max_z}(z)$ (see text for definition) evolution with increasing power, $P = 137.18$ mW (black), 193.5 mW (blue), and 279.7 mW (red); the dot indicates the location Z_S and refers to the maximum of $S_{max_z}(z)$. (b) Numerical maximum transverse steepening $S_{max_z}(z)$ evolution with increasing intensity values $|A|^2 = 5.64 \times 10^6$ (black), $|A|^2 = 7.98 \times 10^6$ (blue), and $|A|^2 = 9.76 \times 10^6$ V^2/m^2 (red), respectively. (c) Experimental evolution of the focusing shocklike distance Z_s (see text for definition) vs injected power P in logarithmic scales showing a power law $Z_s \propto P^{\chi}$, with $\chi = -4/3$ coefficient. (d) Experimental evolution of the transverse position Y_s of the intensity discontinuity (see text for definition) at $z = 1.2$ mm vs injected power P in logarithmic scales showing a power law $Y_s \propto P^{\chi}$, with $\chi = 1/25$ coefficient. All experimental values are averaged over 20 s of dynamics.

driven by the nonlinearity, which leads to a gradient catastrophe. The self-steepening dynamics of our experimental refractive index discontinuity is analyzed, versus propagation, using the previously defined steepness $S_z(y)$. For each z, the maximum value S_{max_z} of $S_z(y)$ is extracted. The typical experimental evolution, during the propagation, of the maximum transverse steepening $S_{max_z}(z)$ for the discontinuity between the ground and high-intensity regions versus power injection P is illustrated in Fig. 4(a). The plotted $S_{max_z}(z)$ profiles correspond to the average of the 100 instantaneous steepness profiles extracted from each frame of the video. In order to avoid noise-induced hot spots and small-scale transverse instabilities in the calculation of S, the Savitzky-Golay algorithm is applied to smooth the signal. It is observed that above $P \approx 135$-mW power, the evolution of $S_{max_z}(z)$ always reveals the occurrence of a maximum [Fig. 4(a)]. It indicates that the jump distribution of the index profile self-steepens during the propagation distance z before "relaxing" or being "regularized" by the dispersive and dissipative medium. This is the characteristic of a shocklike dynamics. Such observation is also reported by Wan *et al.* [30] for the diffraction from an edge but in a *local self-focusing* medium.

Steepness oscillations S_{max_z} along the propagation direction are linked to the corresponding transverse oscillations on the intensity profiles [Fig. 3(d)]. This feature is found in the numerical simulations carried out without noise nor losses ($\epsilon = 0$ and $\beta = 0$) but taking into account for the nonlocal response of the nonlinearity ($K_2 = 6.57 \times 10^{-12}\ N$) [Fig. 4(b)]. These oscillations come from the transverse modulations previously discussed [Figs. 3(a)–3(c)] and their interactions due to nonlocality. The location of the $S(z)$ maximum never occurs above approximately 600 μm propagating distance. The reason is certainly due to losses that overcome nonlinearity for this distance. Such a limitation in the nonlinear effects was already reported in [35]. We extract the longitudinal coordinate Z_s corresponding to the maximum value of $S_{max_z}(z)$ that measures the propagating distance needed for the focusing shocklike dynamics to occur. This distance Z_s moves towards the cell entrance when increasing the initial beam power P as reported for shocks in optical defocusing media (see, e.g., [42]) and in hydrodynamics [20,21]). Indeed, it is known that the shock distance Z_s scales with power P according to the law $Z_s \propto P^{\chi}$, with $\chi = -0.5$ in the hydrodynamic limit. The evolution plot of Z_s versus P for our experimental recordings is drawn in Fig. 4(c). It clearly evidences a power law $Z_s \propto P^{4/3}$ for powers larger than $P \approx 135$ mW [$\ln(P) \approx -4.9$]. Thus, as for shocks in defocusing media, a power law in the form of $Z_s \propto P^{\chi}$ is found. Our $\chi = -4/3$ value is related to the nonlocal nature of our system as shown by Conti *et al.* and Ghofraniha *et al.* in [21,42]. A numerical study would report on the influence of the level of nonlocality on the χ parameter in our system.

VI. CONCLUSIONS

In conclusion, we experimentally show that the propagation of an optical intensity jump discontinuity (Riemann problem) in a *nonlocal focusing* Kerr medium follows a trajectory that bends with the injected beam power P due to the nonlocal nature of the nonlinearity. The transverse beam nonlinear deviation/shift Y_s follows a power law with $Y_s \propto P^{\frac{1}{25}}$. This opens an all-optical route towards beam steering. We also evidenced that the profile of the refractive index self-steepens along propagation and leads to a focusing shock dynamics. It is characterized by a power law, as for self-defocusing local Kerr media, for the shock distance to occur versus the injected beam power P, namely, $P^{-4/3}$. Focusing on the dispersive shock oscillatory structure that should result from the regularization of the discontinuity, it is not observed due to the intrinsic noise that sustains wandering small-scale transverse instabilities. Further investigations are in progress to reduce the stochasticity level in order to experimentally evidence focusing dispersive dam break flow or maybe dissipative flow due to losses.

ACKNOWLEDGMENTS

Authors want to acknowledge S. Trillo and M. Conforti for helpfull discussions. This work has been partially supported by the LABEX CEMPI (ANR-11-LABX-0007) and the Ministry of Higher Education and Research, Hauts de France council and European Regional Development Fund (ERDF) through the Contrat de Projets Etat-Region (CPER Photonics for Society P4S).

[1] I. Freund, Nonlinear Diffraction, Phys. Rev. Lett. **21**, 1404 (1968).

[2] J. D. Joannopoulos, P. R. Villeneuve, and S. Fan, Photonic crystals putting a new twist on light, Nature (London) **386**, 143 (1997).

[3] D. Gomila, R. Zambrini, and G.-L. Oppo, Photonic Band-Gap Inhibition of Modulational Instabilities, Phys. Rev. Lett. **92**, 253904 (2004).

[4] U. Peschel, O. Egorov, and F. Lederer, Discrete cavity solitons, *Nonlinear Guided Waves and Their Applications* (Optical Society of America, Washington, DC, 2004), p. WB6.

[5] S. Koke, D. Träger, P. Jander, M. Chen, D. N. Neshev, W. Krolikowski, Y. S. Kivshar, and C. Denz, Stabilization of counterpropagating solitons by photonic lattices, Opt. Express **15**, 6279 (2007).

[6] N. Marsal, D. Wolfersberger, M. Sciamanna, G. Montemezzani, and D. N. Neshev, Experimental control of pattern formation by photonic lattices, Opt. Lett. **33**, 2509 (2008).

[7] G. A. Askaryan, Effects of the gradient of strong electromagnetic beam on electrons and atoms, Sov. Phys. JETP-USSR **15**, 1088 (1962).

[8] B. Schapers, M. Feldmann, T. Ackemann, and W. Lange, Interaction of Localized Structures in an Optical Pattern-Forming System, Phys. Rev. Lett. **85**, 748 (2000).

[9] S. Barland, J. Tredicce, and M. Brambilla, Cavity solitons as pixels in semiconductor microcavities, Nature (London) **419**, 699 (2002).

[10] A. Piccardi, A. Alberucci, N. Tabiryan, and G. Assanto, Dark nematicons, Opt. Lett. **36**, 1356 (2011).

[11] A. W. Snyder and J. Mitchell, Accessible solitons, Science **276**, 1538 (1997).

[12] D. Buccoliero and A. S. Desyatnikov, Quasi-periodic transformations of nonlocal spatial solitons, Opt. Express **17**, 9608 (2009).

[13] A. Alberucci, C. P. Jisha, and G. Assanto, Breather solitons in highly nonlocal media, J. Opt. **18**, 125501 (2016).

[14] G. A. El', A. V. Gurevich, V. V. Khodorovski, and A. L. Krylov, Modulational instability and formation of a nonlinear oscillatory structure in a "focusing" medium, Phys. Lett. A **177**, 357 (1993).

[15] M. Peccianti, C. Conti, and G. Assanto, Optical modulational instability in a nonlocal medium, Phys. Rev. E **68**, 025602(R) (2003).

[16] W. Królikowski, O. Bang, N. I. Nikolov, D. Neshev, J. Wyller, J. J. Rasmussen, and D. Edmundson, Modulational instability, solitons and beam propagation in spatially nonlocal nonlinear media, J. Opt. B **6**, S288 (2004).

[17] Y. V. Izdebskaya, V. G. Shvedov, P. S. Jung, and W. Krolikowski, Stable vortex soliton in nonlocal media with orientational nonlinearity, Opt. Lett. **43**, 66 (2018).

[18] M. A. Hoefer, M. J. Ablowitz, I. Coddington, E. A. Cornell, P. Engels, and V. Schweikhard, Dispersive and classical shock waves in Bose-Einstein condensates and gas dynamics, Phys. Rev. A **74**, 023623 (2006).

[19] W. Wan, S. Jia, and J. W. Fleischer, Dispersive superfluid-like shock waves in nonlinear optics, Nat. Phys. **3**, 46 (2007).

[20] N. Ghofraniha, C. Conti, G. Ruocco, and S. Trillo, Shocks in Nonlocal Media, Phys. Rev. Lett. **99**, 043903 (2007).

[21] C. Conti, A. Fratalocchi, M. Peccianti, G. Ruocco, and S. Trillo, Observation of a gradient catastrophe generating solitons, Phys. Rev. Lett. **102**, 083902 (2009).

[22] M. Bertola and A. Tovbis, Universality for the focusing nonlinear Schrödinger equation at the gradient catastrophe point: Rational breathers and poles of the tritronquée solution to painlevé I, Commun. Pure Appl. Math. **66**, 678 (2013).

[23] G. A. El and M. A. Hoefer, Dispersive shock waves and modulation theory, Physica D **333**, 11 (2016).

[24] G. Biondini, Riemann problems and dispersive shocks in self-focusing media, Phys. Rev. E **98**, 052220 (2018).

[25] B. Riemann, *Über die Fortpflanzung ebener Luftwellen von endlicher Schwingungsweite, 8* (Abh. Königl. Ges. Wiss. Göttingen, 1860), pp. 43–65.

[26] D. H. Peregrine, Calculations of the development of an undular bore, J. Fluid Mech. **25**, 321 (1966).

[27] J. Fatome, C. Finot, G. Millot, A. Armaroli, and S. Trillo, Observation of Optical Undular Bores in Multiple Four-Wave Mixing, Phys. Rev. X **4**, 021022 (2014).

[28] G. Xu, M. Conforti, A. Kudlinski, A. Mussot, and S. Trillo, Dispersive Dam-Break Flow of a Photon Fluid, Phys. Rev. Lett. **118**, 254101 (2017).

[29] G. Assanto, T. R. Marchant, and N. F. Smyth, Collisionless shock resolution in nematic liquid crystals, Phys. Rev. A **78**, 063808 (2008).

[30] W. Wan, D. V. Dylov, C. Barsi, and J. W. Fleischer, Diffraction from an edge in a self-focusing medium, Opt. Lett. **35**, 2819 (2010).

[31] P. de Gennes and J. Prost, *The Physics of Liquid Crystal* (Oxford University Press, New York, 1993).

[32] I. C. Khoo, *Liquid Crystals, Physical Properties and Nonlinear Optical Phenomena* (Wiley-Interscience, New York, 1995).

[33] X. Hutsebaut, C. Cambournac, M. Haelterman, J. Beeckman, and K. Neyts, Measurement of the self-induced waveguide of a solitonlike optical beam in a nematic liquid crystal, J. Opt. Soc. Am. B **22**, 1424 (2005).

[34] G. Agez, C. Szwaj, E. Louvergneaux, and P. Glorieux, Noisy precursors in one-dimensional patterns, Phys. Rev. A **66**, 063805 (2002).

[35] H. Louis, M. Tlidi, and E. Louvergneaux, Experimental evidence of dynamical propagation for solitary waves in ultra slow stochastic non-local Kerr medium, Opt. Express **24**, 16206 (2016).

[36] N. J. Zabusky and M. D. Kruskal, Interaction of Solitons in a Collisionless Plasma and the Recurrence of Initial States, Phys. Rev. Lett. **15**, 240 (1965).

[37] S. Trillo, M. Klein, G. F. Clauss, and M. Onorato, Observation of dispersive shock waves developing from initial depressions in shallow water, Physica D **333**, 276 (2016).

[38] N. V. Tabiryan and S. R. Nersisyan, Large-angle beam steering using all-optical liquid crystal spatial light modulators, Appl. Phys. Lett. **84**, 5145 (2004).

[39] S. V. Serak and N. V. Tabiryan, Microwatt power optically controlled spatial solitons in azobenzene liquid crystal, Liq. Cryst. X **6332**, 63320Y (2006).

[40] J. Wang, Z. Ma J. Chen, J. Liu, Z. Wang, Y. Li, Q. Guo, W. Hu, and L. Xuan, Observation of optical solitons and abnormal modulation instability in liquid crystals with negative dielectric anisotropy, arXiv:1503.01953.

[41] X. Feng, H. Liu, N. Huang, Z. Wang, and Y. Zhang, Reconstruction of noisy images via stochastic resonance in nematic liquid crystals, Sci. Rep. **9**, 3976 (2019).

[42] N. Ghofraniha, L. S. Amato, V. Folli, S. Trillo, E. DelRe, and C. Conti, Measurement of scaling laws for shock waves in thermal nonlocal media, Opt. Lett. **37**, 2325 (2012).